Journal Pre-proof

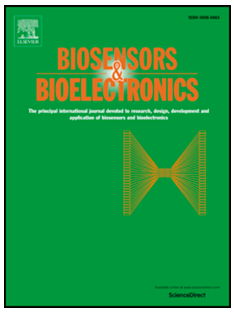

Paper-based electrochemical peptide nucleic acid (PNA) biosensor for detection of miRNA-492: A pancreatic ductal adenocarcinoma biomarker

Maria Moccia, Veronica Caratelli, Stefano Cinti, Biagio Pede, Concetta Avitabile, Michele Saviano, Anna Lisa Imbriani, Danila Moscone, Fabiana Arduini

PII: S0956-5663(20)30365-1

DOI: https://doi.org/10.1016/j.bios.2020.112371

Reference: BIOS 112371

To appear in: *Biosensors and Bioelectronics*

Received Date: 26 March 2020

Revised Date: 28 May 2020

Accepted Date: 6 June 2020

Please cite this article as: Moccia, M., Caratelli, V., Cinti, S., Pede, B., Avitabile, C., Saviano, M., Imbriani, A.L., Moscone, D., Arduini, F., Paper-based electrochemical peptide nucleic acid (PNA) biosensor for detection of miRNA-492: A pancreatic ductal adenocarcinoma biomarker, *Biosensors and Bioelectronics* (2020), doi: https://doi.org/10.1016/j.bios.2020.112371.

This is a PDF file of an article that has undergone enhancements after acceptance, such as the addition of a cover page and metadata, and formatting for readability, but it is not yet the definitive version of record. This version will undergo additional copyediting, typesetting and review before it is published in its final form, but we are providing this version to give early visibility of the article. Please note that, during the production process, errors may be discovered which could affect the content, and all legal disclaimers that apply to the journal pertain.

© 2020 Published by Elsevier B.V.

Journal Pre-proof

Credit Author Statement

Maria Moccia: Conceptualisation of PNA/miRNA experiments, PNA synthesis, Supervision, Funding acquisition, Project administration, Writing - review & editing
Veronica Caratelli: Experimental investigation for the electrochemical part and paper-based sensor fabrication, methodology, data analysis, Writing - review & editing
Stefano Cinti: Conceptualisation of electrochemical experiments and paper-based sensor fabrication, Supervision, Writing - review & editing
Concetta Avitabile: Experimental investigation for PNA synthesis, purification and characterisation
Michele Saviano: Funding acquisition, Project administration, Review & editing
Anna Lisa Imbriani: Funding acquisition, Project administration, Review & editing
Danila Moscone: Funding acquisition, Project administration, Review & editing
Fabiana Arduini: Supervision of electrochemical experiments, Funding acquisition, Project administration, Writing - review & editing

Journal Pre-proof

Journal Pre-proof

Paper-based electrochemical peptide nucleic acid (PNA) biosensor for detection of miRNA-492: a pancreatic ductal adenocarcinoma biomarker

Maria Moccia [1#*], Veronica Caratelli[2#], Stefano Cinti[3], Biagio Pede[2], Concetta Avitabile[1], Michele Saviano[1], Anna Lisa Imbriani[4], Danila Moscone[2], Fabiana Arduini [2,5*]

[1] *Institute of Crystallography, National Research Council, Department of Chemical Sciences and Materials Technology, via G. Amendola 122/O, 70126, Bari, Italy.*

[2]*Tor Vergata University, Department of Chemical Science and Technologies, Via Della Ricerca Scientifica, 00133, Rome, Italy*

[3] *University of Naples "Federico II", Department of Pharmacy, Via Domenico Montesano 49, 80131, Naples, Italy*

[4] *Biochemical Systems International S.p.A. Loc, Palazzo del Pero, 23, 52100 Arezzo, Italy*

[5] *SENSE4MED, Via Renato Rascel 30, 00133, Rome, Italy*

#these authors contributed equally

**Corresponding authors: Fabiana Arduini, email: fabiana.arduini@uniroma2.it; Maria Moccia, email: maria.moccia@cnr.it*

Journal Pre-proof

Abstract

Pancreatic ductal adenocarcinoma is the predominant neoplastic disease of the pancreas and it represents the fourth most frequent cause of death in cancer-related disease, with only 8% of survivors after 5-year to the diagnosis. The main issues of this type of cancer rely on fast progress (i.e. 14 months from T1 to a T4 stage), nonspecific symptoms with delay in diagnosis, and the absence of effective screening strategies. To address the lack of early diagnosis, we report a cost-effective paper-based biosensor for the detection of miRNA-492, which is recognised as a biomarker for pancreatic ductal adenocarcinoma. To design a miniaturised, sensitive, and robust paper-based platform, an electrochemical sensor was screen-printed on office paper previously wax-patterned via wax-printing technique. The paper-based sensor was then engineered with a novel and highly specific peptide nucleic acid (PNA) as recognition element. The formation of PNA/miRNA-492 adduct was evaluated by monitoring the interaction between the positively charged ruthenium (III) hexamine with uncharged PNA and/or negatively charged PNA/miRNA-492 duplex by

differential pulse voltammetry. The paper-based biosensor provided a linear range up to 100 nM, with a LOD of 6 nM. Excellent selectivity towards one- and two-base mismatches (1MM, 2MM) or scrambled (SCR) sequences was highlighted and the applicability for biomedical analyses was demonstrated, measuring miRNA-492 in undiluted serum samples.

Keywords: serum, pancreatic ductal adenocarcinoma, ruthenium (III) hexamine, screen-printing, wax-printing.

Journal Pre-proof

Introduction

In 2018 in Europe, ca. 3 million new cases of cancer were forecasted, observing ca. 2 million dead. Among several cancer types, breast, lung and prostate ones are the most common, and a high rate of mortality has been observed for lung (388,000 deaths), colorectal (243,000), breast (138,000), and pancreatic (128,000) cancer (Ferlay et al. 2018). The pancreatic ones are classified in two main groups, namely exocrine and neuroendocrine tumours. The former group originates from exocrine cells designated to the production of key enzymes for digestion; the latter one affects the neuroendocrine cells, which produce hormones for controlling the normal functions of the body (Kleeff et al., 2016). Among exocrine tumours, the most common one is the pancreatic ductal adenocarcinoma (PDAC), which originates in the epithelial cells of glandular structures and accounting for more than 90% of all pancreatic malignances (Adamasca et al. 2017). PDCA is sometimes called the "silent disease" because it is characterised by a silent progress of primary cancer growth or metastatic diffusion before clinical symptoms (Vincent et al. 2011), thus early diagnosis and treatment represent great challenge to clinicians (McGuigan et al. 2018; Moutinho-Ribeiro et al. 2019). Nowadays the most common tools to diagnose PDAC are computed tomography or ultrasound endoscopy, but these methods require expensive instrumentation and skilled personnel, avoiding a prompt diagnosis, and thus affecting the PDAC management. Actually, several tumor biomarkers have been investigated in blood for monitoring the disease progression and therapeutic response such as TPA/TPS, CA242, CA 494, CA 19-9, but only CA 19-9 has been approved by FDA. However, its average sensitivity (79%) and specificity (82%) are only considered moderate for PDCA screening (Huang et al. 2014; Poruk et al. 2013). To address the challenge of early diagnosis, prognosis, and smart monitoring of treatment effectiveness, liquid biopsy has paving the way for a new concept of analysis in biomedical field. Indeed, liquid biopsy has been established as one of the top 10 emerging technologies in 2017 by the World Economic Forum because it can *mark a step forward in the fight against cancer*. This technology relies on the non-invasive revealing of circulating-tumor biomarkers in blood/serum, e.g. circulating tumour DNA (ctDNA), mRNA, miRNA, exosomes, and circulating tumor cells (CTCs) (Mattox et al. 2019). It provides a wider spectrum of information when compared to tissue biopsy, as well as fast feedback related to disease progression or resistance to treatment.

Among these biomarkers, miRNAs are non-coding RNA molecules encompassing 19-25 nucleotides, which regulate gene expression at post-transcriptional level (Bartel 2009). These tiny nucleic acids are able to regulate cell differentiation, development and homeostasis in health and

pathophysiological disorder in disease (Gebert et al. 2019). Many researches have evidenced that an aberrant expression of miRNA is highly correlated with the development of several diseases including cancer (Adams et al. 2014). For instance, the overexpression of miRNA-210, miRNA-155, miRNA-196a, and miRNA-21 has been found in PDCA patients' serum, demonstrating their potentiality to discriminate PDCA (Wang et al. 2009; Brunetti et al. 2015). Serum miRNAs are usually measured by quantitative polymerase chain reaction (qPCR) with high sensitivity and selectivity, but it requires laboratory set-up and skilled personnel. For a reliable and cost-effective detection by unskilled personnel, point of care devices have opened a new route in clinical diagnoses: several examples are present in literature. miRNA-10b was detected in exosome and residual plasma of blood samples down to 1 aM using a duplex-specific nuclease-assisted dual-SERS biosensor based on hybridisation with the complementary DNA probes (Pang et al. 2019). Joshi et al. (2014) reported a solid-state localised surface plasmon resonance sensor modified with gold nanoprisms and single-stranded DNA probes for detecting miRNA-10b and miRNA-21 down to fM range in 40% bovine plasma and 40% human plasma. Beside these biosensors based on optical transduction, the use of electrochemical detection gathered huge attention by scientific and industrial community for their capability to work in complex matrices like blood as well as for requiring miniaturised transducer, allowing for handheld devices. In this overall scenario, Guo et al. developed a gold-based bulk biosensor immobilising a DNA oligonucleotide capture probe to measure miRNA-196a. Thanks to an enzymatic cyclic signal amplification, this biosensor was able to quantify miRNA-196a with a linear range from 0.05 fM to 50 pM and a detection limit of 15 aM. The accuracy was evaluated by measuring plasma samples spiked with different biomarker concentrations, namely 0.05 fM, 5 fM and 500 fM, obtaining recovery values comprised between 97.6% and 102.2%, thus demonstrating the reliability of the developed biosensor (Guo et al. 2018).

To develop a miniaturised analytical tool, screen-printed electrodes possess all the requirements, being miniaturised, cost-effective and allowing the analysis using few µL of sample. Zeng et al. (2017) developed a 16-channel screen-printed gold electrode array for the detection of miRNA-21, miRNA-155, miRNA-196a, and miRNA-210 by means of tetrahedral DNA nanostructures immobilised on the gold electrode, reaching a detection limit of 10 fM. The reliability of the developed biosensor was assessed in serum, demonstrating its capability to discriminate pancreatic cancer patients from healthy controls.

Beside DNA oligonucleotide capture probes, recently another biocomponent has been exploited in the design of smart biosensor, thanks to its i) higher affinity/specificity between PNA and RNA when compared to DNA and RNA, ii) higher thermal stability than DNA/RNA (PNA is uncharged), iii) higher chemical stability, and iv) resistance to enzymatic cleavage in serum and in cellular

Journal Pre-proof

extracts (Demidov et al. 1994). In details, PNAs are nucleic acid analogues able to bind complementary DNA/RNA sequences following Watson-Crick base pairing (Nielsen et al. 1991). PNA has an uncharged backbone composed of N-(2-aminoethyl)glycine motif (*aeg*) where the four natural nucleobases are linked through a methylene carbonyl group (Figure S1). The neutral backbone confers a greater stability to the PNA-RNA and PNA-DNA complexes in respect to the natural counterparts (Nielsen 2004, Nielsen 2010). In addition, a single mismatch in the middle of a PNA/DNA complex causes a higher drop of melting temperature compared to DNA/DNA one (15°C instead of 4°C), thus demonstrating an improved selectivity of PNA in respect to DNA (Ratilainen et al. 2000). All these features make PNA an outstanding candidate as antisense, antigene (Saarbach et al. 2019), miRNA targeting molecules (Moccia et al., 2016; Piacenti et al., 2019), as well as capture probe in diagnostic applications (Saadati et al. 2019). For instance, Fu et al. developed a biosensor based on a gold electrode modified with PNA and target-catalysed hairpin assembly with redox tags for simultaneous detection of miRNA-21 and miRNA-155 in human cancer cells, with detection limits of 2.49 and 11.63 fM, respectively (Fu et al. 2020). Jolly et al. reported the development of a PNA based biosensor for the detection of miRNA-145 using a gold electrode as platform to immobilise a thiolated PNA. The electrochemical detection of miRNA-145 following the duplex formation allowed to reach a detection limit down to 0.37 fM (Jolly et al. 2016).

In this work, we reported the first paper-based electrochemical PNA biosensor for the detection of miRNA-492, which is suggested as biomarker for PDCA (Lin et al. 2014; Pei et al. 2017). Compared to the polyester and alumina-based screen-printed electrodes, paper-based electrodes have numerous advantages such as the sustainability and the capability to be used for a cost-effective fabrication of microfluidic pattern. Indeed, the paper is an ecofriendly material that is incinerated after the measurement, reducing the waste management (Cinti et al. 2019). In addition, the use of paper as support to print the electrodes allows for a cheap fabrication microfluidic pattern thanks to management of the flow without external pumps, delivering a device that match the ASSURED criteria (Affordable, Sensitive, Specific, User-friendly, Rapid and robust, Equipment-free and Deliverable to end-users) established by WHO (Kosack et al. 2017).

Materials and Methods

2.1 Reagents and Equipment

Chloroauric acid ($HAuCl_4$), sodium borohydride, sodium citrate, sodium chloride, sodium dihydrogen phosphate idrate (NaH_2PO_4 H_2O), sodium hydrogen phosphate (Na_2HPO_4), 6-mercapto-

Journal Pre-proof

1-hexanol (C6-OH), and tris(2-carboxyethyl)phosphine hydrochloride (TCEP), hexaammineruthenium(III) chloride $Ru(NH_3)_6Cl_3$ were purchased from Sigma-Aldrich (St.Louis, MO, USA). All the electrochemical measurements were carried out using a portable potentiostat (PalmSens, Netherlands) equipped with a multiplexer for 8 cells and connected to a laptop.

2.2 Synthesis of PNA

For the synthesis of PNA, Fmoc-PAL-PEG-PS resin supplied by Applied Biosystem was used. The HOBT activators and HBTU were purchased from Novabiochem, while piperidine, DIPEA, acetic anhydride, and TFA were purchased from Biosolve. The N, Methyl-morpholine and Fmoc-Ahx-OH were purchased from Sigma-Aldrich company. The anhydrous solvents for the synthesis of PNAs (DCM, DMF) were provided by the J.T.Baker company. Fmoc-PNA-cytosine(Bhoc)-OH, Fmoc-PNA-thymine-OH, Fmoc-PNA-guanine-(Bhoc)-OH, Fmoc-PNA-adenine(Bhoc)-OH were provided by Panagene while Fmoc-Cys (trt)-OH from Iris Biochem. The analyses and purification of the products were carried out by high pressure reverse phase liquid chromatography (RP-HPLC). Analytical analyses and purification of PNA oligomers were performed on HPLC equipped with UV detector and autosampler, Agilent 1100 Hewlett Packard. A Phenomenex Jupiter 5 μm C18 300Å (4.6 x 250 mm) column was used at a flow of 1 mL/min. LC-MS analyses were conducted using a Phenomenex Jupiter 5 μm C18 300Å column (150x460 nm) Surveyor series HPLC, coupled with a Thermo Finnigan mass spectrometer equipped with an electrospray source (MSQ model). Solid phase synthesis of PNA oligomers was performed on a Fmoc-Pal-Peg-PS resin, with a functionalisation degree of 0.16 mmol/g on a 4 μmol scale, employing a protocol reported in literature (Avitabile et al. 2010). The synthesis consists of repetitive cycles of deprotection, coupling and acetylation, at room temperature. To improve the efficiency of the coupling reaction, double couplings were performed on G and A monomers. For the removal of Fmoc group, a solution of 20% piperidine in DMF was employed for 7 minutes, followed by a wash in DMF for 50 seconds. The coupling was carried out using a 0.22 M solution of PNA monomer (5 eq.) in DMF, a solution 0,20 M of HOBt/HBTU in DMF (5 eq.) and 100 μl of a mixture of NMM (N-N-methyl morpholine, 5 eq.) in pyridine for 20 minutes. 100 μL of monomer were activated with 100 μL of the HOBt and HBTU solutions and at this solution, 100 μL of a solution of NMM in pyridine was added. The mixture was added to the resin for 20 minutes at room temperature and then removed by filtration. The resin was washed with DMF twice. Then, the acetylation of the unreacted amino groups by treatment with a mixture of acetic anhydride/2,6, Lutidine/DMF 5/6/89 v/v/v for 5 minutes was carried out, followed by two washes in DMF. At the end of the synthesis, the resin was washed with DMF, DCM, Et_2O and dried under vacuum. The conjugate Cys-Ahx-AntimiR492 was

obtained adding Fmoc-Ahx-OH and Fmoc-Cys (trt)-OH at the N terminus of PNA oligomers still immobilised on the resin. Fmoc-Ahx-OH (2.5 eq) was preactivated for 5 min with a solution of HOBt and HBTU (2.49 eq.) 0.45 M in DMF and NMM (3.5 eq.). The solution was incubated on the resin for 45 min under stirring at room temperature and the coupling was repeated twice to assure a complete functionalization. After acetylation and deprotection of the Fmoc group, the amino acid Fmoc-Cys (trt)-OH was anchored with the same procedure: 2.5 eq. of Fmoc-Cys(trt)-OH was preactivated for 5 min with a solution of HOBT and HBTU (2.49 eq) 0.45 M in DMF and NMM (3.5 eq). The solution was incubated on the resin for 45 min under stirring at room temperature and the coupling was repeated twice to assure a complete functionalisation. At the end of the synthesis, the resin was washed with DMF, DCM, Et_2O and dried under vacuum. The conjugates were cleaved from the resin and deprotected treating the resin with a TFA/H_2O/EDT/TIS solution (94/2.5/2.5/1) for 90 minutes at room temperature and under stirring. TFA was removed from samples under nitrogen flow and the oligomers were precipitated with cold ethyl ether, washed three times with ethyl ether, vacuum-dried, and lyophilised. The purification of the conjugates was carried out through reverse phase HPLC on a semi-preparative column, using a gradient of acetonitrile (0.1% TFA) in H_2O (0.1% TFA) from 5 to 50% in 30 minutes. The purified products by characterised by ESI-TOF mass spectrometry. Cys-Ahx-AntimiR-PNA 492: Cys-Ahx- aagaatcttgtcccgcaggtcct (Da): Found: 6421.6224; $[M+3H]^{3+}$: 2142.5408; $[M+4H]^{4+}$: 1606,4056; $[M+5H]^{5+}$: 1285.3244;Calculated: 6421.3286; $[M+3H]^{3+}$: 2142.4429; $[M+4H]^{4+}$: 1606,3321; $[M+5H]^{5+}$: 1285.2657 (Figure S2). RNA sequences were purchased from Biomers.net the polymer factory Ulm (Germany).

Journal Pre-proof

2.3 Circular dichroism and circular dichroism thermal denaturation experiments

Circular dichroism (CD) experiments were carried out on a Jasco J-810 Spectropolarimeter equipped with a NesLab RTE111 peltier. CD spectra were recorded in a 1 cm cuvette (Hellma) at 5 °C and 95 °C in the 320-200 nm range using duplexes 3 μM concentration in phosphate buffer 10 mM pH=7, 100 mM NaCl. Duplexes were annealed by warming up at 90 °C for 5 minutes and slowly cooling down to 5 °C and kept at least 12 h at this temperature. Thermal denaturation experiments were carried out using 3 μM duplexes in phosphate buffer 10 mM pH=7, 100 mM NaCl at a 1 °C/min scanning speed and recording the signal at 260 nm. The other experimental parameters were 100 nm min^{-1}scanning speed, 50 mdeg sensitivity, 16 s time constant, 1 nm

bandwidth. Each spectrum was obtained from an average of three accumulations, subtracting the spectrum of the solvent. The spectra were reported as optical density (mdeg).

2.4 Synthesis of gold nanoparticles (AuNPs) dispersion

First of all, glassware and magnetic stir bar used in this synthesis were cleaned in aqua regia (HCl/HNO_3 3:1 (v/v)), rinsed in distilled water, and subsequently cleaned with piranha solution (H_2SO_4/H_2O_2 7:3 (v/v)), and rinsed again with distilled water before use. Then, AuNPs were obtained in a round flask at room temperature (RT), mixing 9 mL of distilled water with 1 mL of 0.01 g/mL $HAuCl_4$ and 2 mL of 0.01 g/mL sodium citrate. After 1-minute stirring, 0.5 mL of 20 mM sodium borohydride were added drop-by-drop. The solution was left under stirring and in dark condition for 24 h. The gold nanoparticles dispersion was then stored at 4 °C.

2.5 Production of the paper-based SPEs

The first step in the production of paper-based SPEs was the design of the pattern using a drawing software (Adobe Illustrator). The pattern was printed on office paper sheet (80 g/m^2, Fabriano Copy 2) using a wax printer (ColorQube 8580 Xerox). The paper-based substrate was patterned with two layers of wax. The first layer, the green one, was treated in oven at 100 °C for 2 min. The wax penetrated the paper structure producing hydrophobic areas. Then, a second wax layer was printed (black layer) without being cured in the oven. This top layer aims at delimitating the testing area. This configuration was previously optimised for obtaining a more durable platform during the measurement (Cinti et al. 2018). After that, the paper was ready to manually screen-print the three-electrode system (screen-printed electrodes, SPEs). A silver/silver chloride ink (Electrodag 4038 SS) was used to print the pseudo-reference electrode, while a graphite ink (Electrodag 421) was used to print the counter and working electrodes. The conductive inks were applied through masks with the desired patterns and they were all purchased from Acheson (Italy).

2.6 Preparation of the paper-based sensor

8 µL of AuNPs were drop-cast onto the working electrode, and after drying, the probe was immobilised following a protocol reported in literature (Xiao et al. 2007). The first step is the reduction of 100 µM PNA (50 mM phosphate buffer pH=7, 150 mM NaCl in RNase free water) in

presence of 10 mM TCEP for 1 h. The resulting solution was then diluted to the selected concentration (in the range of nanomolar) to be immobilised onto the AuNPs-SPEs. 20 µL drop of the probe was placed onto the working electrode area for 1 h at RT in a humid chamber. SPEs were gently washed with distilled water and incubated in a humid chamber with 2 mM C6-OH to passivate the empty spaces onto the working electrode. The last step was washing away with distilled water the unbound C6-OH from the SPEs, then they were left overnight at 4 °C in the working buffer solution (50 mM phosphate buffer containing 150 mM NaCl, pH=7). The entire platform was conceived as disposable sensor, as in the case of glucose strip used every day by diabetic patients at worldwide level, especially because of the choice of paper as support, in order to develop an eco-friendly and sustainable device which can be easily disposed after its use (e.g. by incineration), reducing the environmental impact of printed electrochemical sensors.

2.7 Measurement of miRNA target

For the measurement of miRNA target, eight SPEs were inserted into the multiplexer connected to the portable potentiostat. 100 µL of working buffer, prepared in RNase free water (50 mM phosphate buffer containing 150 mM NaCl, pH 7) were added onto the electrochemical cells. Then, the concentration of the target to be analysed (in the range of nM) was added into the 100 µL of buffer. After 20 minutes, 5 µL of the redox mediator, $Ru(NH_3)_6Cl_3$, were added to the working solution and the current was recorded after further 20 minutes (Cinti et al., 2020) using as electrochemical technique Differential Pulse Voltammetry (DPV) (E begin = -0.1 V, E end = -0.5 V, E step = 0.005 V, E pulse = 0.05 V, T pulse = 0.05 V and Scan rate = 0.05 V/s (vs. Ag/AgCl as reference electrode).

For the optimisation experiments and response curves, the signal change was plotted against the concentration of the target analysed using the signal of paper-based SPE modified with gold nanoparticles and PNA in presence of $Ru(NH_3)_6^{3+}$ as background current, which was subtracted to the signal of the sensor in presence of the target.

Result and Discussions

3.1 PNA/miRNA-492 binding characterisation in solution

The binding of PNAs with DNA and RNA targets is stronger compared to DNA/DNA or RNA/RNA binding (Nielsen et al. 1991, Chakrabarti et al. 1999). This enhanced binding affinity is

partially ascribed to the uncharged nature of PNAs. Indeed, the duplexes formed by PNA/DNA or PNA/RNA hybrids lack the electrostatic repulsion present in DNA/DNA or RNA/DNA duplexes, delivering a very stable complex with high binding affinity (Jensen et al. 1997, Schwarz et al. 1999, Chakrabarti et al. 1999). Before immobilising the PNA bioreceptor on the electrode surface, the interaction between the *ad hoc* synthesised PNA sequence and the target miRNA-492 was assessed by CD, obtaining information about affinity of PNA/RNA hetero duplex and secondary structure of the duplex. In Figure S3, the overlayed CD profile in case of single strand miRNA-492 (red line) and the complex PNA/miRNA-492 (1:1) (blue line) was reported. In case of duplex PNA/miRNA-492, a positive maxima at *ca*. 260 and 220 nm together with negative minimum at *ca*. 240 nm and a small negative band between 290 and 300 nm was observed demonstrating the binding between PNA/miRNA-492, being this CD profile typical of PNA/RNA heteroduplex (Corradini et al. 2012). Furthermore, the position of the peaks suggests the presence of a helical structure resembling the A-form RNA (Gray et al. 1981). In addition, the stability of the duplex was measured by CD melting denaturation experiment for 1:1 complex, after the annealing procedure, which revealed a melting temperature (T_m) of 92 °C. On the contrary, T_m of the native duplex RNA-miRNA-492, which was estimated by Oligo-Calculator software (http://biotools.nubic.northwestern.edu/OligoCalc.html), was 59.2 °C (salt adjusted) and 78.4 (Nearest neighbor method), thus lower when compared to PNA/miRNA492 duplex, confirming the higher affinity of PNA sequences than the natural counterparts (Nielsen et al. 1991, Jensen et al. 1997, Schwarz et al. 1999, Chakrabarti et al. 1999).

3.2 Paper-based PNA configuration and detection mechanism

The paper-based device was conceived by combining a customised PNA probe and a nanostructured working electrode surface on a wax printed layer on paper for delivering an eco-designed electrochemical paper-based platform. The paper was modified with two layers of wax to delimitate a testing zone where the reaction between the PNA probe immobilised onto working electrode surface and miRNA-492 in 100 µL solution happened, delivering a drop sensitive measurement. To tailor the orientation of PNA, the graphite-based working electrode surface was modified with gold nanoparticles for supplying gold anchor points and control PNA immobilisation through the thiol tail of *ad hoc* synthesised PNA. For an effective duplex formation between PNA and miRNA-492, PNA probe was designed to be fully complementary to miRNA-492 with anti-parallel orientation (3’□end RNA facing the PNA N□term) (Figure S1), because this configuration confers an improved stability of the duplex compared to the parallel orientation (Nielsen et al.

Journal Pre-proof

1999). After the synthesis of the PNA portion, an aminohexanoic acid (Ahx) was introduced as spacer between the PNA and the successive cysteine residue. A thiol group, employing a cysteine residue was introduced at the N terminus of the PNA oligomer and used to anchor the PNA to AuNP-SPE. For the detection of miRNA-492, a *signal on* strategy was selected (Das et al. 2016), allowing for a more sensitive quantification in respect to the *signal off*, due to an increase of the output when an input is produced, namely current and target concentration. The principle of detection relies on the use of an external positively charged redox mediator, i.e. $Ru(NH_3)_6^{3+}$, that is added to the working solution to monitor the formation of PNA/miRNA-492 duplex. Indeed, the redox mediator (positively charged) accumulates at the working electrode because of the electrostatic attraction to the negatively charged PNA/miRNA-492 adduct. Thus, in presence of the target analyte (negatively charged), an increase of signal is observed as shown in Figure 1. To evaluate the suitability of this method, a first experiment was carried out using 5 mM $Ru(NH_3)_6^{3+}$ as redox probe with the following platforms i) paper-based SPE modified with only gold nanoparticles, ii) paper-based SPE modified with gold nanoparticles and PNA, iii) paper-based SPE modified with gold nanoparticles, PNA, and target. In addition, a paper-based SPE modified with gold nanoparticles and PNA in buffer solution was tested in absence of $Ru(NH_3)_6^{3+}$. The measurement in presence of $Ru(NH_3)_6^{3+}$ using paper-based SPE modified with only gold nanoparticles did not give any response (Figure S4, green line) because $Ru(NH_3)_6^{3+}$ is not able to be adsorbed in quantitative way on this surface. The blank signal was also observed in case of paper-based SPE modified with gold nanoparticles and PNA (Figure S4, black line), but tested in buffer solution in absence of $Ru(NH_3)_6^{3+}$. However, the experiment with $Ru(NH_3)_6^{3+}$ and paper-based SPE modified with gold nanoparticles and PNA gave a defined peak ascribed to aspecific adsorption process of $Ru(NH_3)_6^{3+}$ on PNA (Figure S4, blue line). Moreover, in presence of paper-based SPE modified with gold nanoparticles, PNA, and target, a higher signal was observed due to the additional electrostatic interaction of $Ru(NH_3)_6^{3+}$ with negatively charged RNA-based target strand (Figure S4, red line), demonstrating the effectiveness of the principle for the detection of miRNA target.

3.3 Optimisation of PNA probe

A relevant step in the fabrication of the sensor is represented by the probe immobilization because an ordered layer allows a homogenous surface that improves the target recognition, and the signal intensity is proportional to the amount of the immobilised probe. Briefly, high probe density allows

Journal Pre-proof

for a high signal output but low sensitivity, while a low probe density allows for a higher probability of binding but low signal output; thus, a compromise between signal output and binding moiety was evaluated. In our format, the density optimisation was carried out evaluating different concentrations of PNA solution as well as the immobilisation time of the probe on working electrode surface. The first study was focused on evaluating the response of sensors modified with 25, 50, 100 and 200 nM PNA probe, in presence of 50 nM miRNA-492 as target (Fig. 2). As reported in Figure 2A, the concentration of 100 nM gave the highest signal variation (33%) and the lowest RSD (18%), thus this value was selected for further studies. Once identified the optimal probe concentration, the effect of the immobilisation time was investigated by evaluating the response of the sensor after the exposure to 100 nM of PNA solution for 0.5, 1, 2 and 4 h. As shown by the experimental results, the maximum signal change is observed when 1 h is chosen for immobilising PNA probe. The use of longer times does not produce better results in terms of signal, while a slight decrease of the resulting signal is revealed. Moreover, the chosen time allowed the obtainment of the best RSD of 11%, compared to the other conditions, thus it was chosen as the optimal time (Fig. 2B).

3.4 pH effect

The PNA/miRNA-492 interactions are based on hydrogen bonds thus the evaluation of the optimal working solution pH is necessary. In addition, the final application in physiological matrices of this platform makes necessary the study of pH effect on the signal output investigating the range between pH 7 and pH 8. As reported in Figure 2C, although the intensity of pH 7.4 was consistent with the highest signal variation, its repeatability was ca. 2-fold worse than the one obtained working with pH 7. For this reason, pH 7 was chosen as the optimal pH for carrying out the detection.

3.5 Selection of hexamine ruthenium concentration

The concentration of the redox mediator is also another crucial parameter able to affect the sensitivity of the measurement. In this case, an optimal concentration of redox mediator should be identified because a lower concentration could be reflected in a low amount of the mediator electrostatically attracted by PNA/RNA probe, resulting in low recorded current. On the contrary, a

Journal Pre-proof

too high redox probe could arise in issue during the removal of its excess, thus increasing the background signal at low target concentration. This study was carried out by varying the redox mediator from 1.25 to 10 mM, as shown in Figure 2D. As highlighted in Figure 2D, both 2.5 and 10 mM concentrations produced a signal variation, however 5 mM gave the highest signal variation (43%) and the lowest RSD% (ca. 8%), thus this concentration was selected for the further studies.

3.6 Study of the time and temperature effect on PNA/miRNA-492 binding

Considering the final development of a point of care test for miRNA-492 detection, the binding process between probe and target represents a significant step. Compared to the time for immobilising the probe, the study of the binding time has a direct implication towards the effective duration of the test. Specifically, the time requested to form the probe-target adduct is strictly dependent on the nature and length of sequences, and on the *probe + target* ←→ *probe-target* equilibrium, and in literature is reported that the formation of duplex structures for *ca*. 20 bp targets requires about 15-20 min (Patterson et al. 2010; Cinti et al. 2018). Thus, after having covered the strip with the sample, the probe-target interaction time needs to be carefully optimised to obtain the best compromise in term of sensitivity, repeatability, and time of analysis. This optimisation was performed by waiting for 10, 15, 20, 40 and 60 min after applying 100 nM target, as reported in Figure 3A. According with the experimental observations, a time of 20 min gave the maximum signal variation (40%) with the lowest RSD% associated (7%), and this value was selected for the rest of the work. Following this study, the last optimisation regarded the evaluation of the temperature on the ability of forming the probe-target adduct. Considering the thermodynamic nature of the binding, the temperature could impact the final detection. The effect of temperature was evaluated between 4 and 37 °C in presence of 100 nM target, as shown in Figure 3B. Results suggested that the optimal temperature for the binding event between probe and target is 25 °C in terms of intensity of the signal and repeatability (RSD % equal to 10 %), thus this value was selected.

3.7 Analytical features

Once optimised all main parameters affecting the sensitivity of the paper-based strip, the analytical characterisation was performed measuring the signal due to different concentrations of miRNA-492 in standard solution. The optimised platform was evaluated with 100 nM of probe in presence of target concentrations ranging from 10 to 1000 nM (Figure 4A). In detail, the response curve

Journal Pre-proof

obtained in buffer solution was characterised by a linear range between 50 to 100 nM, described by the following equation y = (-0.40 ± 0.05) + (0.0122 ± 0.0006) x, R^2=0.987 (Figure 4A, inset). The detection limit was calculated as the concentration of miRNA-492 able to give a signal change equal to 3 times the standard deviation of the blank (absence of the target) and it was found equal to 19 nM.

3.8 Selectivity study

Successively, the platform selectivity was tested in presence of sequences differing from the target even for a single base. The sequences tested presented: 1 mismatch in the central zone of the sequence, (5'-AGGACCUGCGGUACAAGAUUCUU-3', 1MM); 2 mismatch in the central zone of the sequence, (5'-AGGACCUGCGGUCCAAGAUUCUU-3', 2MM,); 1 mismatch in the 5' end of the sequence, (5'-UGGACCUGCGGGACAAGAUUCUU-3', 1MM-5'), 1 mismatch in the 3' end of the sequence, (5'-AGGACCUGCGGGACAAGAUUCUC-3', 1MM-3'), and a fully random sequence (5'-CAAU UUCAUAAAGUGGAGCCUCC-3', RNA-SCR). All the selectivity experiments were carried out in presence of 80 nM of the above described sequences, and all the results were compared to the detection of 80 nM of the native fully complementary miRNA target (5'-AGGA CCUGCGGGACAAGAUUCUU-3'). The results reported in Figure 5A demonstrated that the presence of mismatches had not a significant effect on the signal variation. In fact, while the presence of miRNA-492 produced a variation of 70% with respect to the blank, the occurrence of interferences was only responsible of a 5-15% variation. In addition, to underline the selectivity of the biosensor proposed, the platform was tested at different concentrations of these interfering sequences. The following sequences 1MM, 2MM, 1MM-, 1MM-3' and RNA-SCR were tested in the concentration range comprised between 10 and 1000 nM. The biosensor showed excellent selectivity towards the target analyte miRNA-492, because no signal change in presence of other sequences even at higher concentrations, characterised by one mismatch or fully random sequence was observed (Fig. 5A, inset). Moreover, interference studies regarding substances present in the serum were performed. 100 nM miRNA-492 were measured in presence of different interferent compounds namely albumin, urea, glucose, and uric acid at level of 0.435 mM, 16.7 mM, 27.8 mM, and 0.595 mM, respectively. The concentrations were chosen in agreement with the literature (Osawa et al. 2005). The results showed that the compounds have slight interfering effects (Fig. 5B), demonstrating satisfactory selectivity considering that this device was conceived as point of care and not as reference method.

3.9 Serum analyses

The suitability of this platform for measurements in bodily fluids, such as blood serum, is guaranteed by the "blindness" of electroanalysis in presence of coloured matrices that often limits the application of colorimetric assays. For this study, blood serum was chosen as the real matrix to evaluate the real application of the platform. Serum was provided by volunteers, and after having confirmed the absence of miRNA-492 target (within the detection limit of the method), undiluted serum was spiked with different levels of target. A response curve was obtained in undiluted serum in presence of miRNA-492 in the 10-100 nM range (Fig. 4B) and it was characterised by a linearity between 50 to 100 nM described by the following equation $y = (-0.30 \pm 0.05) + (0.0116 \pm 0.0007)$ x, R^2=0.993 (Fig. 4B, inset). It is interesting to observe how even in presence of serum (complex matrix) the electrochemical platform is able to give satisfactory results in term of detection limit (22 nM). These features are consistent with the possibility of this platform to be adopted as a potent tool for rapid pancreatic cancer screening at the point of care.

4. Conclusion

In this work, the first satisfactory application of a fully-paper based electrochemical strip for pancreatic ductal adenoma carcinoma (PDCA) detection was described. In particular, the detection of miRNA-492 was optimised through a multi-disciplinary perspective including the selection of a sustainable substrate (office paper), the engineering of the probe, and the evaluation of the target-probe binding. The adoption of PNA probes, in combination with a "signal on" architecture for the sensing mechanism, allowed for avoiding issues related to stability and pH effect, which often represent the bottle-neck when DNA/RNA are adopted as the probes. In less than 1 h, the electrochemical strip was able to detect miRNA-492 down to 10 nM in few microliters of sample, and it has displayed a good selectivity in presence of interfering species with only one mismatch along the sequence. The sensing tool was positively applied in spiked undiluted serum samples with satisfactory results. The features of this sensor in terms of easiness to use, time of production, sensitivity, and applicability in complex matrix namely serum, demonstrated the suitability of this sensor when compared with other electrochemical sensors reported in literature (Table 1) as well as its promising application for future clinical analyses. The preliminary results reported in this work open to a plethora of applications, not only in the clinical field: in fact, the strategy of coupling low-cost materials and specific engineered probes is highly extendible to other matrices. In particular, in the rising field of liquid biopsy, the ultimate electrochemical paper-based tool could represent a potent instrument to give rapid answers to both patients and physicians, reducing the time gap between disease and treatment.

Acknowledgments

M.M. and M.S. like to acknowledge H2020-PON-MISE 2014/2020 - Project. n. F/050013/03/X32. The PRIN 2017 prot. 2017Y2PAB8_004 project "Cutting Edge Analytical Chemistry Methodologies and Bio-Tools to Boost Precision Medicine in Hormone-Related Diseases" is also acknowledged for funding.

Figure captions

Figure 1. Schematic representation of the paper-based electrochemical PNA platform for the detection of miRNA-492.

Figure 2. A) Optimisation of the PNA concentration. Concentrations tested in the range 25-200 nM. Immobilisation time of probe = 1 h. Inset: current signal at the paper-based SPE in absence (black dashed line) and in presence (blue solid line) of 50 nM miRNA-492 with 100 nM PNA immobilised on the working electrode surface. **B)** Optimisation of the PNA immobilisation time. 30 min, 1, 2, 4 h were tested using 100 nM PNA, 100 nM miRNA-492. Inset: current signal at the paper-based SPE in absence (black dashed line) and in presence (orange solid line) of 100 nM miRNA-492 with 100 nM PNA immobilised on the working electrode surface at 1 h of PNA immobilisation time. **C)** Study of pH effect. pH values tested were 6.8, 7, 7.4, 8 using 100 nM PNA, 1 h PNA immobilisation time, 100 nM miRNA-492. Inset: current signal at the paper-based SPE in absence (black dashed line) and in presence (green solid line) of 100 nM miRNA-492 with 100 nM PNA immobilised on the working electrode surface, pH = 7. **D)** Optimisation of the $Ru(NH_3)_6^{3+}$ concentration. Concentration tested in the range between 1.25 to 10 mM using 100 nM PNA, 1 h PNA immobilisation time, 100 nM miRNA-492, binding time 20 minutes. Inset: current signal at the paper-based SPE in absence (black dashed line) and in presence (yellow solid line) of 100 nM miRNA-492 with 100 nM PNA immobilised on the working electrode surface using 5 mM $Ru(NH_3)_6^{3+}$. All the optimisations were carried out with reagents prepared in phosphate buffer solution 50 mM + 100 mM NaCl, pH = 7 (n=3), using 2.5 mM $Ru(NH_3)_6^{3+}$ and 50 nM miRNA-492, binding time = 20 minutes. All measurements were carried out using paper-based SPE with printed Ag/AgCl pseudoreference.

Figure 3. A) Study of the time effect on the PNA/miRNA-492 binding. Different binding times were tested in the range between 10 min to 2 h using 100 nM PNA, 1 h PNA immobilisation time, 100 nM miRNA-492, 5 mM $Ru(NH_3)_6^{3+}$. Inset: current signal at the paper-based SPE in absence (black dashed line) and in presence (purple solid line) of 100 nM miRNA-492 with 100 nM PNA immobilised on the working electrode surface, binding time = 20 minutes. **B)** Study of the temperature effect on the PNA/miRNA-492 binding. Three different binding temperatures were tested: 4, 25, 37 °C using 100 nM PNA, 1 h PNA immobilisation time, 100 nM miRNA-492, 5 mM $Ru(NH_3)_6^{3+}$, binding time = 20 minutes. Inset: current signal at the paper-based SPE in absence (black dashed line) and in presence (cyan solid line) of 100 nM miRNA-492 with 100 nM PNA immobilised on the working electrode surface, binding temperature = 25 °C. All the optimisations were carried out with reagents prepared in phosphate buffer solution 50 mM + 100 mM NaCl, pH =

7 (n=3). All measurements were carried out using paper-based SPE with printed Ag/AgCl pseudoreference.

Figure 4. A) Response curve obtained testing different concentrations of miRNA-492 in the range between 10 and 1000 nM prepared in phosphate buffer solution 50 mM + 100 mM NaCl, pH = 7 using 100 nM PNA, 1 h PNA immobilisation time, 5 mM $Ru(NH_3)_6^{3+}$, binding time = 20 minutes (n=3). Inset: response curve in the linear range comprised between 50 and 100 nM using 100 nM PNA, 1 h PNA immobilisation time, 5 mM $Ru(NH_3)_6^{3+}$, binding time = 20 minutes (n=3). **B)** Response curve obtained testing different concentrations of miRNA-492 in the range between 10 and 1000 nM prepared in un-diluted serum using 100 nM PNA, 1 h PNA immobilisation time, 5 mM $Ru(NH_3)_6^{3+}$, binding time = 20 minutes (n=3). Inset: response curve in the linear range comprised between 50 and 100 nM using 100 nM PNA, 1 h PNA immobilisation time, 5 mM $Ru(NH_3)_6^{3+}$, binding time = 20 minutes (n=3). All measurements were carried out using paper-based SPE with printed Ag/AgCl pseudoreference.

Figure 5. A) 80 nM of different sequences were tested to evaluate the selectivity of the platform: native fully complementary miRNA target (NS), 1 mismatch in the central zone of the sequence (1MM), 2 mismatch in the central zone of the sequence (2MM), 1 mismatch in the 5' zone of the sequence (1MM-5'), 1 mismatch in the 3' zone of the sequence (1MM-3'), and a fully random sequence (RNA-SCR). All the experiments were carried out in presence of 100 nM PNA, 1 h PNA immobilisation time, 5 mM $Ru(NH_3)_6^{3+}$, binding time = 20 minutes (n=3). Inset: 10, 50, 100, 1000 nM of NS, 1MM, 2MM, 1MM-3', 1MM-5' and RNA-SCR sequence were tested using 100 nM PNA, 1 h PNA immobilisation time, 5 mM $Ru(NH_3)_6^{3+}$, binding time = 20 minutes (n=3). **B)** The effect of 0.435 mM albumin, 16.7 mM urea, 27.8 mM glucose, and 0.595 mM uric acid was tested using 100 nM PNA, 1 h PNA immobilisation time, 100 nM miRNA-492, 5 mM $Ru(NH_3)_6^{3+}$, binding time = 20 minutes (n=3).

Table 1. Some examples of electrochemical sensors for miRNA detection.

Journal Pre-proof

References

Adamska, A., Domenichini, A., Falasca M., 2017. Int. J. Mol Sci. 18, E1338.

Adams, B.D., Kasinski, A.L., Slack, F. J. 2014. Curr. Biol., 24, R762-R776.

Avitabile, C., Moggio, L., D'Andrea, L.D., Pedone, C., Romanelli, A. 2010. Tet. Lett. 51, 3716–3718.

Bartel, D.P., 2009. Cell. 136, 215-233.

Brunetti, O., Russo A., Scarpa, A., 2015. Oncotarget 6(27), 23323–23341.

Chakrabarti, M.C, Schwarz, F.P., 1999. Nucleic Acids Res. 27, 4801-4806.

Cinti, S., Proietti, E., Casotto, F., Moscone, D., Arduini, F., 2018. Anal. Chem. 90(22), 13680-13686.

Cinti, S., Moscone, D., & Arduini, F., 2019. Nat. Protoc. 14(8), 2437-2451.

Cinti, S., Cinotti, G., Parolo, C., Nguyen, E. P., Caratelli, V., Moscone, D., Arduini, A., Merkoçi, A., 2020. Anal. Chem. 92(2), 1674-1679.

Corradini, R., Tedeschi, T., Sforza, S., Marchelli, R., 2012. Electronic circular dichroism of peptide nucleic acidd and their analogoues in: Berova, M.m Polavarapu, P.L., Nakanishi, K., Woody, R.W. (Eds.), Comprehensive Chiroptical Spectroscopy: Applications in Stereochemical Analysis of Synthetic Compounds, John Wiley & Sons Inc.

Das, J., Ivanov, I., Sargent, E. H., Kelley, S.O., 2016. J. Am. Chem. Soc. 138, 11009-11016.

Demidov, V.V., Potaman, V.N., Kamenetskii, M.D.F., Egholm, M., Buchart, O., Sonnischsen, S.H., Nielsen, P.E., 1994. Biochem. Pharmacol. 48, 1310-1313.

Dong, H., Jin, S., Ju, H., Hao, K., Xu, L.P., Lu, H., Zhang, X., 2012. Anal. Chem. 84(20) 8670-8674.

Ferlay, J., Colombet, M., Soerjmataram, I., Dyba, T.A., Randi, G., Bettio, M., Gavin, A., Visser, O., Bray F., 2019. Eur. J. Cancer 103, 356-387.

Fu, P., Xing, S., Xu, M., Zhao, Y., Zhao, C., 2020. Sens. Actuators B Chem. 305, 127545.

Gao, Z., Yang, Z., 2012. Anal. Chem. 78, 1470-1477.

Gebert, L.F.R., MacRae I.J., 2019. Nat. Rev. Mol. Cell Biol. 20, 21-37.

Gray, D. M., Liu, J., Ratliff, R. L., Allen, F. S., 1981. Biopolymers 20, 1337−1382.

Guo, J., Yuan, C., Yan, Q., Duan, Q., Li, X., Yi, G., 2018. Biosens. Bioelectron. 105, 103-108.

Huang, Z., Liu F., 2014. Tumor Biol.,35, 7459-7465.

Jensen, K.K., Orum, H., Nielsen, P.E., Norden, B., 1997. Biochemistry 36, 5072-5077.

Joshi, G.K., Deitz-McElyea, S., Johnson, M., Mali, S., Korc, M., Sardar R., 2014. Nano Lett. 14, 6955-6963.

Kosack, C.S., Page, A. L., Klatser P.R., 2017. Bulletin of the World Health Organization 95, 639-645.

Lin, M.S., Chen, W.C., Huang, J.X., Gao, H.J., Sheng, H.H., 2014. Int. J. Clin. Exp. Med. 7 5226-5234.

Lusi, E.A., Passamano, M., Guarascio, P., Scarpa, A., Schiavo, L., 2009. Anal. Chem. 81(7), 2819-2822.

Mattox, A.K., Bettegowda, C., Zhou, A., Papadopoulos, N., Kinzler, K.W., Vogelstein B., 2019. Sci. Tran. Med. 11, eaay1984.

McGuigan, A., Kelly, P., Turkington, R.C., Jones, C., Coleman, H.G., McCain R.S., 2018. World J. Gastroenterol. 24, 4846-4861.

Moccia, M., Adamo, M.F.A., Saviano, M., 2016. Artificial DNA: PNA & XNA 5, e1107176, 1-15.

Moutinho-Ribeiro, P., Macedo, G., Melo, S.A., 2019. Front. Endocrinol. 9, 779.

Nielsen, P.E., Egholm, M., Berg, R.H, Buchardt, O., 1991. Science 254, 1497-1500.

Nielsen, P.E., Egholm, M., 1999. Curr. Issues Mol. Biol. 1, 89-104.

Nielsen, P.E., 2004. Mol. Biotechnol. 26 (3), 233-248.

Nielsen, P.E., 2010. Chem. Biodivers. 7 (4), 786-804.

Osawa, S., Kariyone, K., Ichihara, F., Arai, K., Takagasa, N., Ito, H., 2005. Clin. Chim. Acta 351(1-2), 65-72.

Pang, Y., Wang, C., Lu, L.C., Wang, C., Sun, Z., Xiao, R., 2019. Biosens. Bioelectron. 130, 204-213.

Patterson, A., Caprio, F., Vallée-Bélisle, A., Moscone, D., Plaxco, K.W., Palleschi, G., Ricci, F., 2010. Anal. Chem. 82, 9109−9115.

Pei, Z., Liu, S.M., Huang, J.T., Zhang, X., Yan, D., Xia, Q., C. Ji, W. Chen, X. Zhang, J. Xu, J. Wang, 2017. Oncotarget 8, 22616-22624.

Peng, Y., Jiang, J., Yu, R., 2014. Anal. Methods 6, 2889

Journal Pre-proof

Piacenti, V., Langella, E., Autiero, I., Nolan, J.C., Piskareva, O., Adamo, M.F.A., Saviano, M., Moccia, M., 2019. Bioorg. Chem. 91, 103165.

Pohlmann, C., Sprinzl, M., 2010. Anal. Chem., 82(11), 4434-4440.

Poruk, K.E., Gay, D.Z., Brown, K., Mulvihill1, J. D., Boucher, K.M., Scaife, C.L., Firpo, M.A., Mulvihill, S. J., 2013. Curr. Mol. Med. 13, 340–351.

Ratilainen, A., Holmen, E., Tuite, P.E. Nielsen, Norden, B., 2000. Biochemistry 39, 7781–7791.

Saadati, A., Hassanpoura, S., La Guardia, M., Mosafer, J., Hashemzaeiei, M., Mokhtarzadeha, A., Baradarana, B., 2019.Trend. Anal. Chem. 114, 56-68.

Saarbach, J., Sabale, P.M., Winssinger, N., 2019. Cur. Opin. Chem. Biol. 52, 112–124.

Schwarz, F.P., Robinson, S., Butler, J.M., 1999. Nucleic Acids Res. 27(24), 4792–4800.

Vincent, A., Herman, J., Schulick, R., Hruban, R.H., Goggins, M., 2011. Lancet 378, 607–620.

Wang, J., Chen, J., Chan, P., LeBlanc, A., Li, D., Abbruzzese, J.L., Frazier, M.L., Killary, A.M., 2009. Sen Cancer Prev. Res. 2, 807–813.

Wittung, P., Nielsen, P. E., Buchardt, 0., Engholm, M., Norden, B., 1994. Nature 368, 561-563.

Xiao, Y., Lai, R.Y., Plaxco, K.W., 2007. Nat. Protoc. 2, 2875-2880.

Zeng, D., Wang, Z., Meng, Z., Wang, P., San, L., Wang, W., Aldalbahi, A., Li, L., Shen, J., Mi, X., 2017. ACS Appl. Mater. Interfaces 9, 24118-24125.

Journal Pre-proof

Type of sensor	Technique	Working electrode	Probe	Reagents needed for the measurement	Signal detection	Principle of method	Electrode preparation time	LOD	Sample	Comments	Ref.
Isoniazid-capped OsO_2 nanoparticles-based sensor	Amperometry	ITO electrode	Oligonucleotide probe	PBS (pH 8.0) containing hydrazine	Oxidation of hydrazine catalysed by OsO_2	After hybridisation with periodate-treated miRNA, the nanoparticle tags were brought to the electrode through a condensation reaction to chemically amplify the signal	12-13 h	80 fM	-	The method requires a chemical ligation-based miRNA assay	Gao and Yang, 2006
Gap hybridization assay-based sensor	Amperometry	Gold electrode	RNA probe	pAPB (enzymatic substrate)	Oxidation of pAP, the product of hydrolysis of pAPB catalysed by reporter enzyme EST2	The hybridisation assay requires the immobilized capture ODN, miRNA (target), EST2-ODN conjugate, and complementary RNA probe	20 h	2 pM	-	The method requires the generation of a continuous base stacking, in a coaxial helix formed by four hybridisation components, for generating a significant signal	Pohlmann and Sprinzl, 2010
Oligonucleotide encapsulated Ag-NCs-based sensor	DPV	Ag-NCs modified Au electrode	MB probe	PBS (pH 7.0) containing H_2O_2	Reduction of H_2O_2 catalysed by AgNCs	After hybridisation between MB probe and the target and functional probe, the oligonucleotide encapsulated Ag-NCs are brought to the electrode surface and produce a detection signal, in response to H_2O_2 reduction	18 h	67 fM	-	The method requires a functional oligonucleotide probe consisting of recognition sequence for hybridization and template sequence for in situ synthesis of Ag-NCs	Dong et al., 2012
Streptavidin–	DPV	Gold	DNA probe	α-naphtyl phosphate	Oxidation of	After the hybridisation	13 h	99.2 fM	-	The method requires a	Peng et al., 2014

gold nanoparticles and enzymatic amplification-based biosensor		electrode		(enzymatic substrate)	naphtol, the product of reaction between biotin-ALP and 1-NP	between miRNA and DNA probe, biotin group was introduced into the duplex by the incorporation of biotin-11-dUTP. SA-AuNPs are used as linker to bind Biotin-ALP to duplex				primer extension reaction carried out by DNA polymerase and dNTPs	
Electrochemical genosensor	DPV	Graphite electrode	DNA probe	-	Oxidation of guanine	After hybridisation between miRNA and inosine substitute capture probe, guanine is oxidised on WE surface	3 h	5 nM	-	The SPEs require a pretreatment before probe electrodeposition onto electrodes surface	Lusi et al., 2009
Paper-based PNA biosensor	DPV	AuNPs modified graphite electrode	PNA probe	$Ru(NH_3)_6^{3+}$	Reduction of $Ru(NH_3)_6^{3+}$	After hybridisation between PNA probe and miRNA, $Ru(NH_3)_6^{3+}$ is added to the working solution	4 h	22 nM	Serum	The method does not require any pre-treament steps of electrodes	This work

Table 1. OsO_2: osmium dioxide; ITO: indium tin oxide; PBS: phosphate buffer solution; Au: gold; p-Aminophenyl butyrate; EST2: esterase 2 enzyme; pAP: p-aminophenol; ODN: oligodeoxynucleotide; AgNCs: silver nanoclusters; DPV: differential pulse voltammetry; MB: molecular beacon; H_2O_2: hydrogen peroxide; Biotin-ALP: biotinylated alkaline phosphatase; 1-NAP: 1-naphthyl phosphate; SA-AuNPs: streptavidin-gold nanoparticles; PNA: peptide nucleic acid; AuNPs: gold nanoparticles; $Ru(NH_3)_6^{3+}$: hexaammineruthenium(III) chloride.

Figures

Figure 1

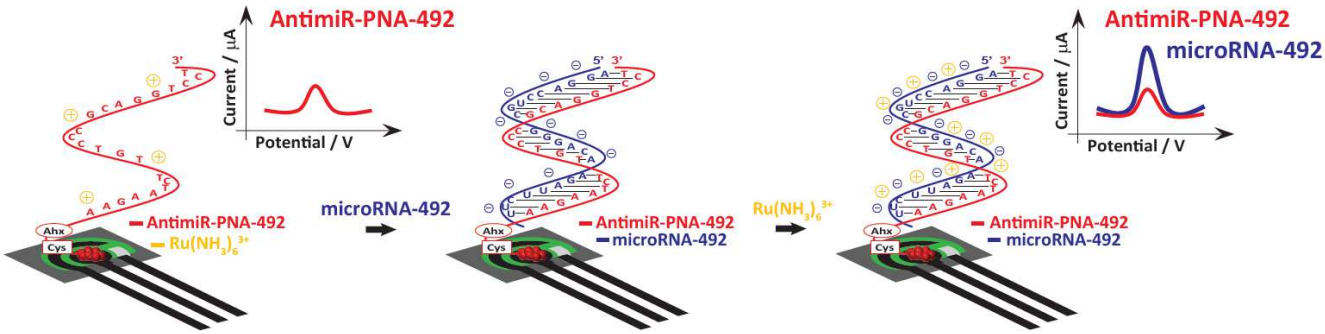

Figure 2

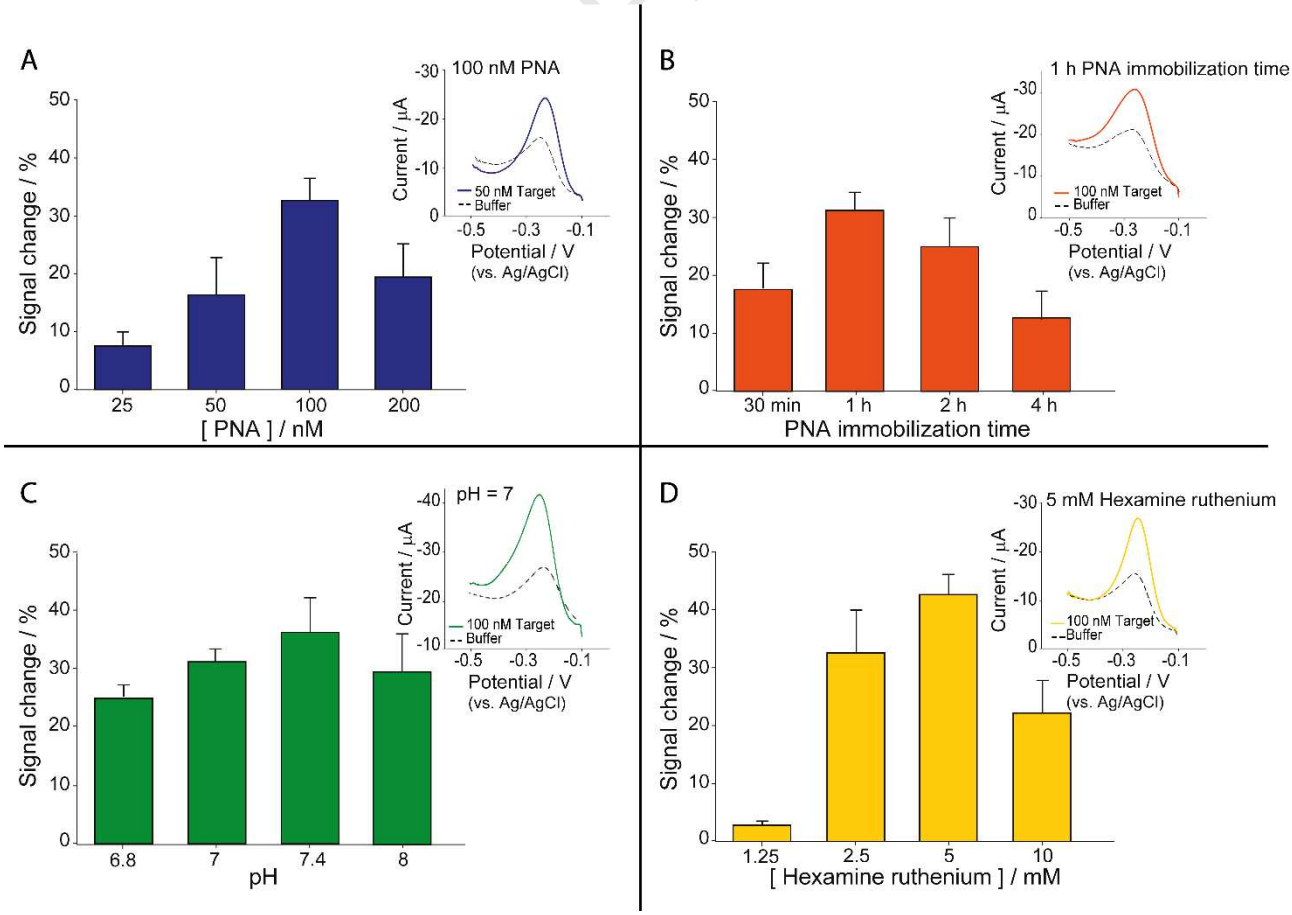

Figure 3

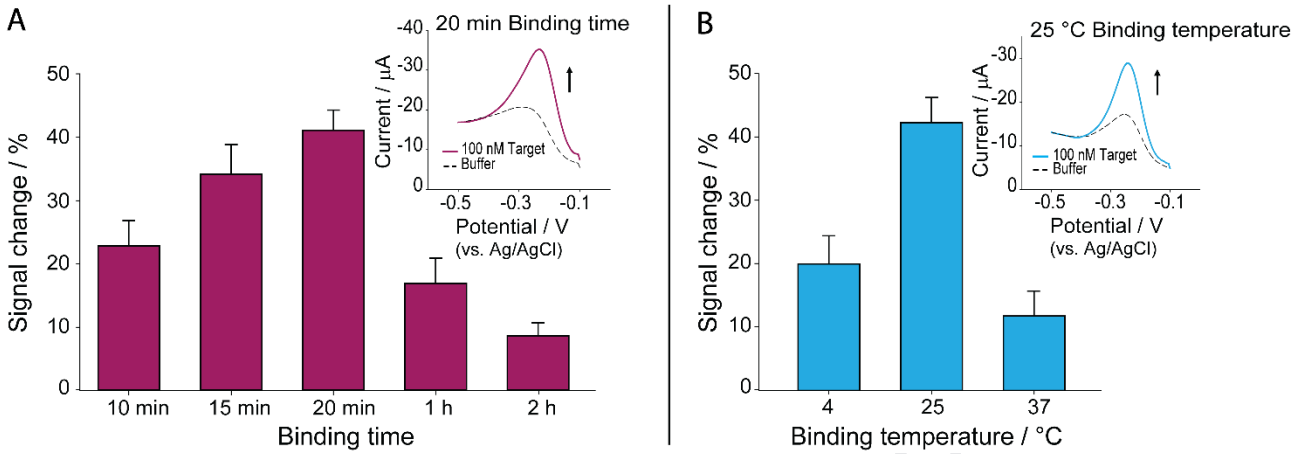

Figure 4

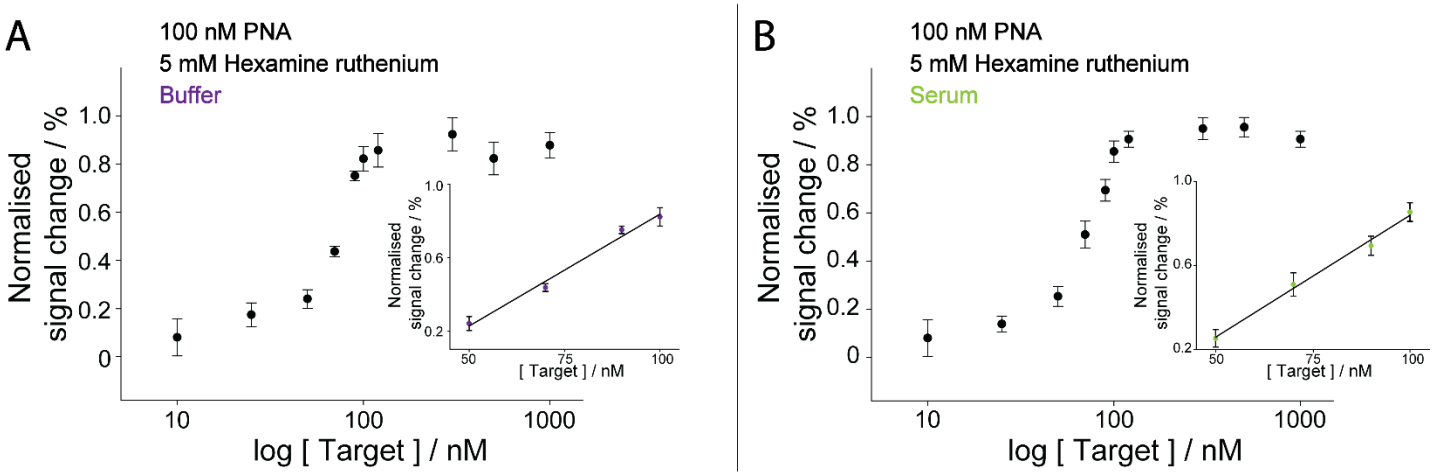

Figure 5

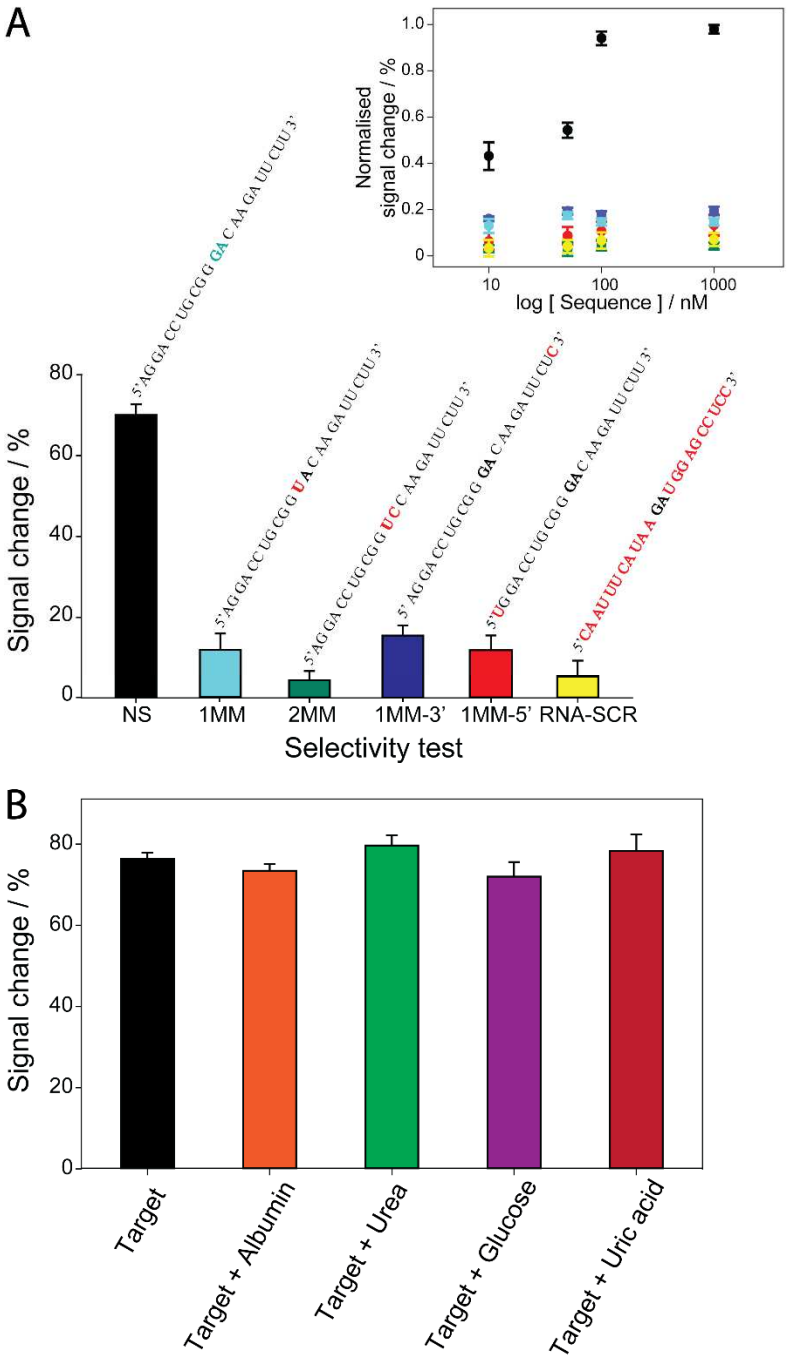
A
Normalised signal change / %
log [Sequence] / nM
Signal change / %
NS
1MM
2MM
1MM-3'
1MM-5'
RNA-SCR
Selectivity test
B
Signal change / %
Target
Target + Albumin
Target + Urea
Target + Glucose
Target + Uric acid

Journal Pre-proof

Highlights

- Paper-based electrochemical peptide nucleic acid (PNA) biosensor for the detection of miRNA-492
- miRNA-492 detection in undiluted serum samples by *signal on* strategy using charged redox mediator
- Wax/screen-printing, paper and nanomaterials for a laboratory-free platform

Journal Pre-proof

Journal Pre-proof

Declaration of interests

☒ The authors declare that they have no known competing financial interests or personal relationships that could have appeared to influence the work reported in this paper.

☐The authors declare the following financial interests/personal relationships which may be considered as potential competing interests:

Journal Pre-proof